Stem Cell Reports
Article

ISSCR

OPEN ACCESS

EZH2 Protects Glioma Stem Cells from Radiation-Induced Cell Death in a MELK/FOXM1-Dependent Manner

Sung-Hak Kim,[1] Kaushal Joshi,[1] Ravesanker Ezhilarasan,[2] Toshia R. Myers,[5] Jason Siu,[1] Chunyu Gu,[1] Mariko Nakano-Okuno,[1] David Taylor,[1] Mutsuko Minata,[1] Erik P. Sulman,[2] Jeongwu Lee,[4] Krishna P.L. Bhat,[3] Anna Elisabetta Salcini,[5] and Ichiro Nakano[1,*]

[1]Department of Neurological Surgery, The James Comprehensive Cancer Center, The Ohio State University, Columbus, OH 43210, USA
[2]Department of Radiation Oncology, The University of Texas, MD Anderson Cancer Center, Houston, TX 77030, USA
[3]Department of Pathology, The University of Texas, MD Anderson Cancer Center, Houston, TX 77030, USA
[4]Department of Stem Cell Biology and Regenerative Medicine, Lerner Research Institute, Cleveland Clinic, Cleveland, OH 44195, USA
[5]Biotech Research and Innovation Centre (BRIC), University of Copenhagen, Ole Maaløes Vej 5, 2200 Copenhagen, Denmark
*Correspondence: ichiro.nakano@osumc.edu
http://dx.doi.org/10.1016/j.stemcr.2014.12.006

SUMMARY

Glioblastoma (GBM)-derived tumorigenic stem-like cells (GSCs) may play a key role in therapy resistance. Previously, we reported that the mitotic kinase MELK binds and phosphorylates the oncogenic transcription factor FOXM1 in GSCs. Here, we demonstrate that the catalytic subunit of Polycomb repressive complex 2, EZH2, is targeted by the MELK-FOXM1 complex, which in turn promotes resistance to radiation in GSCs. Clinically, EZH2 and MELK are coexpressed in GBM and significantly induced in postirradiation recurrent tumors whose expression is inversely correlated with patient prognosis. Through a gain-and loss-of-function study, we show that MELK or FOXM1 contributes to GSC radioresistance by regulation of EZH2. We further demonstrate that the MELK-EZH2 axis is evolutionarily conserved in *Caenorhabditis elegans*. Collectively, these data suggest that the MELK-FOXM1-EZH2 signaling axis is essential for GSC radioresistance and therefore raise the possibility that MELK-FOXM1-driven EZH2 signaling can serve as a therapeutic target in irradiation-resistant GBM tumors.

INTRODUCTION

Glioblastoma (GBM) is the most common primary malignant brain tumor and the median survival of patients is less than 2 years (Brennan et al., 2013). The current standard of therapy involves maximal surgical resection followed by radiotherapy and chemotherapy. However, this treatment strategy fails to eliminate a subset of tumor cells that escape from therapeutic insult and result in tumor recurrence, leading to reduced survival in these patients. A GBM tumor is composed of heterogeneous tumor cell populations that include tumor cells with stem cell properties, termed glioma stem-like cells (GSCs) (Hemmati et al., 2003; Singh et al., 2004). Accumulating evidence indicates that GSCs contribute to radioresistance and subsequent tumor cell repopulation, resulting in recurrent tumors (Bao et al., 2006). Therefore, it is critical to elucidate the molecular mechanisms underlying the radioresistance of GSCs.

Maternal embryonic leucine-zipper kinase (MELK) is a serine/threonine kinase and is abundantly expressed in GBM and various other cancers (Gu et al., 2013; Joshi et al., 2013; Minata et al., 2014; Nakano et al., 2008, 2011). We previously reported that MELK is highly expressed in GSCs and its mRNA expression is inversely correlated with the survival of GBM patients (Gu et al., 2013; Nakano et al., 2008). In addition, short hairpin RNA (shRNA)-mediated MELK elimination induces GSC apoptosis with less inhibitory effects on normal neural progenitor cells (NPCs) (Nakano et al., 2005). Mechanistically, MELK associates with two oncogenic transcription factors (c-JUN and FOXM1) in GSCs, but not their normal counterparts, which explains at least in part the cancer-specific, survival-promoting function of MELK (Gu et al., 2013; Joshi et al., 2013). Nonetheless, the pathophysiological roles of MELK in GSC radioresistance remain elusive.

Polycomb group (PcG) proteins are important epigenetic regulators of embryonic development and the cell fate decision (Aloia et al., 2013). PcG proteins play a crucial role in mediating global transcriptional repression as two large protein assemblies termed Polycomb repressive complex 1 (PRC1) and PRC2 (Aloia et al., 2013; Margueron and Reinberg, 2011). The core components of PRC2 include EZH2 (enhancer of Zeste homolog 2), Suz12 (suppressor of Zeste 12), and EED (embryonic ectoderm development). In particular, EZH2 functions as a lysine methyltransferase, and EZH2-containing PRC2 catalyzes trimethylation of histone 3 at lysine 27 (H3K27me3) (Margueron and Reinberg, 2011). In a wide range of cancers, including GBM, elevated expression of EZH2 is well recognized and its expression is strongly linked to tumor malignancy and invasiveness (Kim et al., 2013; Radulović et al., 2013). Recent studies, including ours (Kim et al., 2013; Lee et al., 2008), suggested that EZH2 plays a critical role in GSC maintenance and GBM propagation similar to the function of MELK in

GSCs. These studies prompted us to speculate that MELK and EZH2 may be involved in the same signaling pathway in GSCs. In this study, we tested the hypothesis that MELK is an upstream regulator of EZH2 signaling to promote GSC survival and resistance to radiation therapy on GBM tumors and GSCs.

RESULTS

MELK and EZH2 Are Colocalized in GBM Cells and Upregulated after Radiation Treatment

To investigate whether MELK and EZH2 could potentially interact, we first performed immunofluorescence and examined their localization. As shown in Figure 1A, MELK$^+$ cells exhibited high immunoreactivity to EZH2 and the two proteins colocalized. A strong correlation between MELK and EZH2 protein expression in GBM tumors was also observed in tissue microarray (n = 76) patient samples and western blot analyses (n = 17) (Figure 1B and Figure S1A). At the mRNA level, a statistically significant correlation between MELK and EZH2 expression was found in high-grade gliomas (HGGs) (Figure 1C). A strong correlation between *MELK* and *EZH2* was also observed when they were examined in three glioma data sets (Freije et al., 2004; Sun et al., 2006; Verhaak et al., 2010; https://tcga-data.nci.nih.gov/docs/publications/gbm_exp/) (Figure S1B). Intriguingly, when expression of MELK and EZH2 was compared between newly diagnosed, untreated GBM tumors and recurrent GBM tumors after failed radiation and chemotherapy, both of these proteins were markedly upregulated in recurrent tumors (Mao et al., 2013; Phillips et al., 2006; http://www.ncbi.nlm.nih.gov/geo/query/acc.cgi?acc=GSE4271) (Figures 1D and S1C). When GBM tumors were divided into two groups based on patient survival time after diagnosis, both *MELK* and *EZH2* were considerably elevated in patients with a worse prognosis (Figure 1E). To corroborate these results with the immunohistochemical findings in recurrent GBM tumors, we irradiated three glioma sphere samples (GBM83, GBM1123, and GBM528) (Mao et al., 2013). We observed a substantial increase in both the mRNA expression and protein levels of MELK and EZH2 in vitro (Figures 1F, 1G, and S1D). Interestingly, postirradiation (post-IR) upregulation of *MELK* and *EZH2* was also observed in nontumorigenic differentiated glioma sphere samples (GBM83 and GBM1123) (Figure S2). In addition, GSC-derived xenograft tumors in mice showed an elevation of these two proteins after IR treatment in vivo (Figure 1H). Collectively, MELK and EZH2 are colocalized in a subset of GBM tumor cells, and both the mRNA and protein expressions of these genes are upregulated in GBM tumors and GSCs after IR.

MELK-Mediated EZH2 Signaling Is Required for GSC Radioresistance

In a recent study (Gu et al., 2013), we demonstrated that MELK downregulation induces a loss of the stem cell phenotype with subsequent tumor cell differentiation and reduced clonogenicity and tumorigenicity in GBM cells. Given the IR-induced substantial upregulation of MELK in GBM spheres, we postulated that MELK may protect against IR-induced GSC death. To test this possibility, we combined IR treatment with MELK overexpression, followed by fluorescence-activated cell sorting (FACS) analysis for cellular apoptosis in GBM83 and GSC23 spheres (Bhat et al., 2013; Mao et al., 2013) using Annexin V and propidium iodide. As expected, MELK overexpression partially restored IR-induced apoptotic populations (Figure 2A). On the other hand, MELK knockdown by shRNA resulted in an increased number of apoptotic cells (Figure S3). Interestingly, when these GBM spheres were pretreated with an EZH2 inhibitor, GSK126, rescue of GBM sphere apoptosis mediated by MELK overexpression was almost completely attenuated (Figure 2A), indicating a possible MELK-mediated EZH2 signaling axis in GSC survival after IR-induced cellular damage, at least in vitro.

Next, we assessed the effect of combining MELK silencing with IR treatment for GBM sphere-derived mouse tumors in vivo. For this experiment, we used luciferase-engineered GSC23 spheres (Bhat et al., 2013). After shMELK infection, dissociated GSC23 spheres were xenografted into mouse brains and treated with fractionated doses of IR (4 × 2.5 Gy) (Figure 2B). Tumor growth was then followed by bioluminescence imaging. Unlike the tumors in control mice with nontarget shRNA, GSC23 sphere-derived tumors treated with MELK knockdown followed by IR displayed substantially reduced sizes at day 42 after xenografting. Subsequently, prolonged survival of tumor-bearing mice by IR was strongly enhanced by MELK silencing in GSC23 spheres (average prolonged survival of 13 days in the shNT [control] group versus 27 days in the shMELK group; Figure 2C). Taken together, these data suggest that post-IR MELK upregulation promotes tumorigenesis and propagation in vivo.

MELK and EZH2 Have Evolutionarily Conserved Functions in Radioprotection

MELK and EZH2 are highly conserved in both mammalian and nonmammalian multicellular species. Therefore, we asked whether the MELK and EZH2 homologs found in the nematode *Caenorhabditis elegans* also function in IR-induced DNA damage responses. The *C. elegans* germline is an established model for studying DNA damage response mechanisms as well as stem cell proliferation and survival in vivo (Garvin et al., 1998). The adult

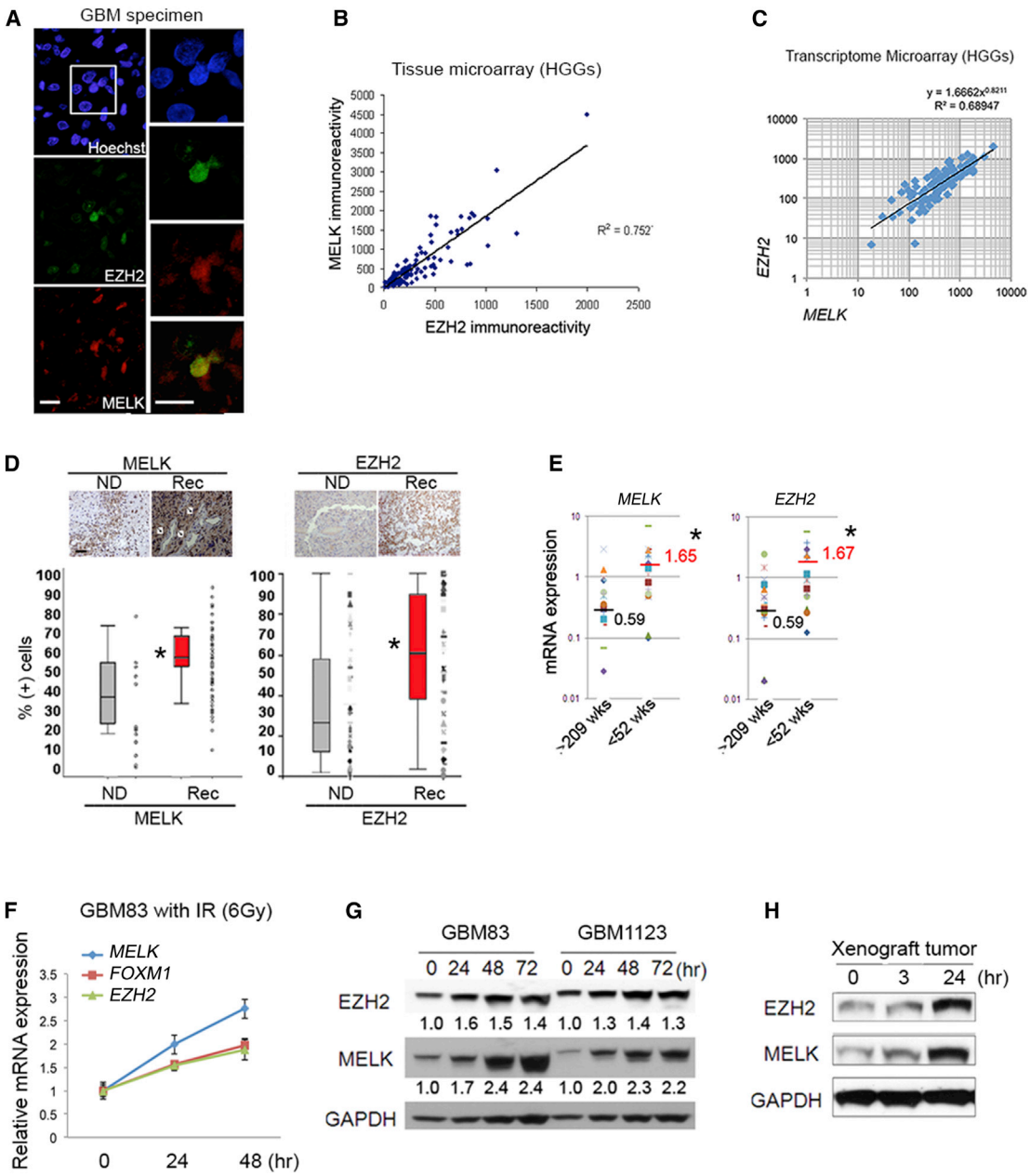

Figure 1. MELK and EZH2 Are Colocalized in GBM Cells and Upregulated after Radiation Treatment

(A) Immunostaining for EZH2 (green) and MELK (red) in GBM tumors. Nuclei were stained with Hoechst (blue). Scale bar represents 25 μm.

(B) Correlation of MELK and EZH2 protein expression by microarray analysis of HGGs (n = 76).

(C) Correlation of *MELK* and *EZH2* mRNA expression by microarray analysis of HGGs (n = 76).

(D) Immunohistochemistry for MELK and EZH2 in newly diagnosed (ND, n = 65) or recurrent (Rec, n = 41) tumors, with corresponding quantification of cells (%) immunoreactive against each protein. Bottom two panels: quantification of $MELK^+$ and $EZH2^+$ cells in ND and Rec tumors analyzed with ImageJ software. Scale bar represents 50 μm. Asterisk (*) indicates statistical significance by Student's two-tailed t test; *$p < 0.05$. Arrow indicates postradiation vasculosclerosis.

(E) *MELK* and *EZH2* mRNA expression in patients with good (>209 weeks survival, n = 19) versus poor (<52 weeks survival, n = 17) prognosis in the Phillips et al. (2006) data set. Asterisk (*) indicates statistical significance by Student's two-tailed t test; *$p < 0.05$.

(F) Relative mRNA expression levels (normalized to *GAPDH*) of *MELK*, *FOXM1*, and *EZH2* in GBM83 glioma spheres at 24 and 48 hr after 6 Gy radiation treatment. Data are represented as means ± SD of triplicate experiments.

(legend continued on next page)

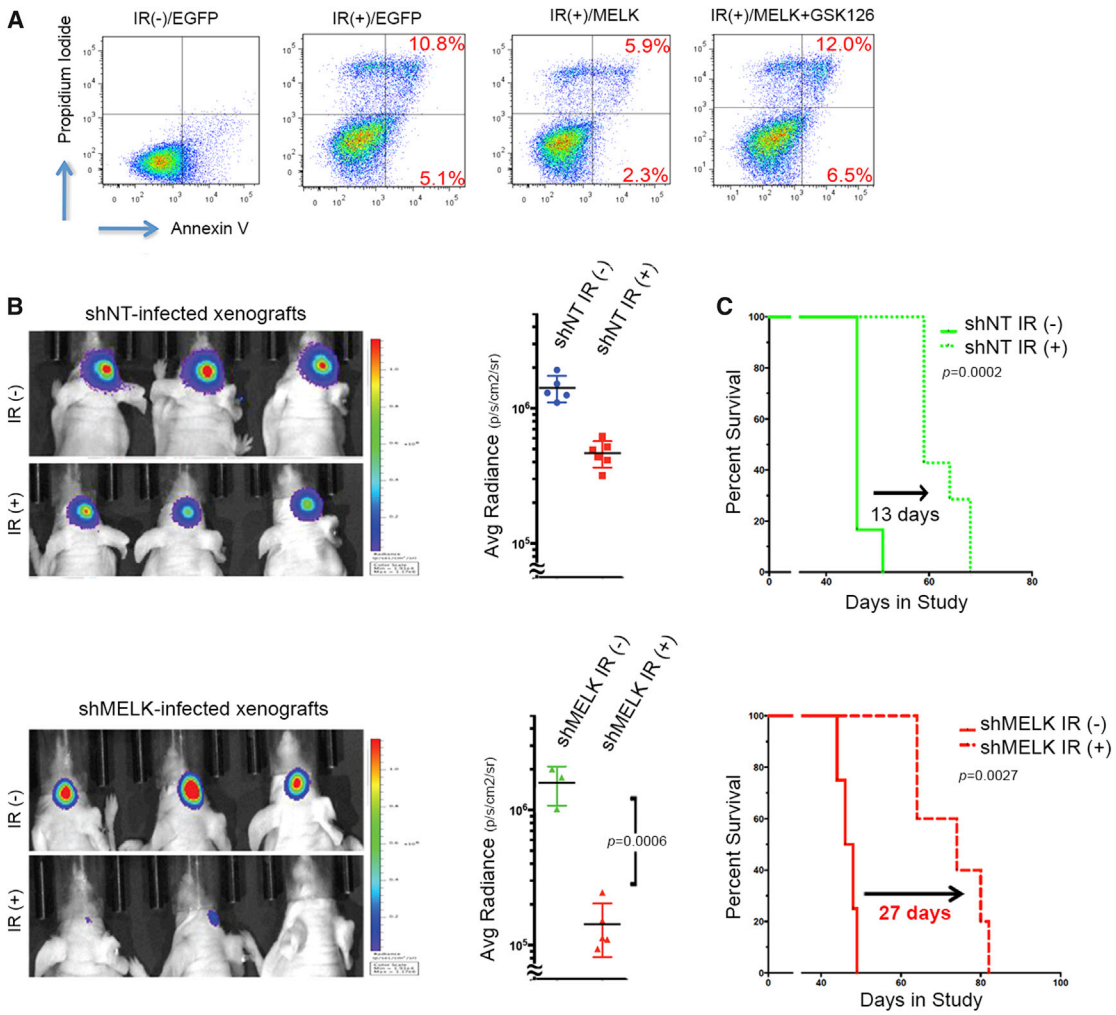

Figure 2. MELK-Mediated EZH2 Signaling Is Required for GSC Radioresistance

(A) Flow-cytometric analysis of GBM spheres for Annexin V and propidium iodide. Left panel: nonirradiated, EGFP-overexpressing control. Left middle panel: irradiated, EGFP-overexpressing control. Right middle panel: irradiated, MELK-overexpressing GSCs. Right panel: irradiated, MELK-overexpressing GSCs treated with the EZH2 inhibitor GSK126.

(B) Bioluminescence imaging (left panel) and average radiance (right panel) of tumor growth after infection with shNT (nontarget control, n = 5) or shMELK (n = 5), followed by treatment with or without fractionated doses of radiation (4 × 2.5 Gy). Error bar indicates ± SEM; p values were calculated by Student's two-tailed t test.

(C) Kaplan-Meier survival curves of tumor-burden mice with the indicated treatments as shown in (B).

See also Figure S3.

hermaphrodite germline consists of two symmetrical U-shaped tubular structures in which a population of proliferating mitotic cells creates a stem cell niche at the distal end (Figure 3A). The mitotic cells migrate proximally from the distal end, transition into meiosis and progress through the stages of prophase I, and eventually form oocytes at the proximal end of the tube. Under physiological conditions, approximately half of the germ cells undergo apoptosis, which is detectable in late pachytene and early diplotene.

(G) Western blot analysis of EZH2 and MELK in GBM83 and GBM1123 glioma spheres at 24, 48, and 72 hr after 6 Gy radiation treatment. The values below the blots indicate the relative expression levels of EZH2 and MELK protein in comparison with GAPDH.

(H) Western blot analysis of EZH2 and MELK in GSC-derived tumors at 0, 3, and 24 hr after in vivo IR.

See also Figures S1 and S2.

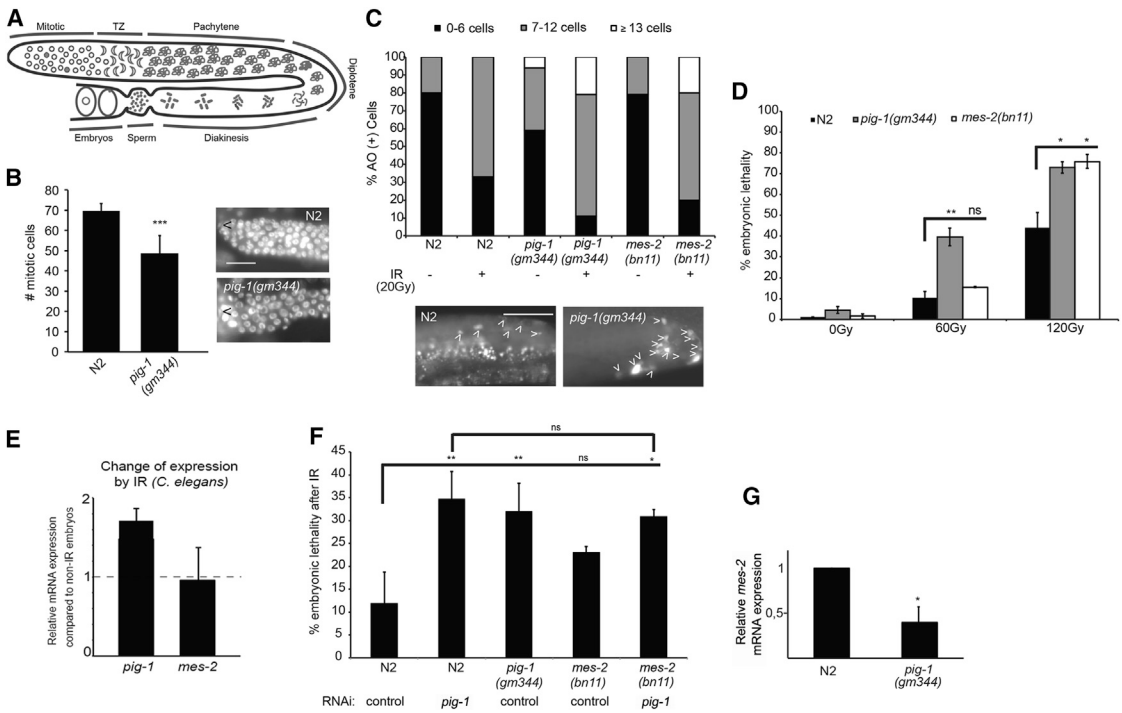

Figure 3. MELK/EZH2 Functions in Radioprotection Are Evolutionarily Conserved

(A) Schematic of *C. elegans* germline migration and development. The mitotic region is located at the distal end. Meiosis I begins at the transition zone (TZ) and as the nuclei progress proximally, they enter pachytene, diplotene, and diakinesis. Oocytes mature in diakinesis before being fertilized by sperm and becoming embryos.

(B) Quantification of mitotic cells in wild-type (N2) or *pig-1* mutant. Two independent experiments were used for the quantification. Data are represented as means ± SD; ***p < 0.001. Representative images of the mitotic region stained with DAPI are shown on the left. Arrowhead indicates distal tip.

(C) Proportion of AO^+ cells in wild-type (N2), *pig-1*, or *mes-2* mutants with or without treatment with 20 Gy IR. Young adult worms were treated with IR, rescued overnight, and then stained with AO. At least 15 gonads were counted for each strain and condition. The *mes-2 (bn11)* strain is either homozygous or heterozygous for the *mes-2* allele. Two independent experiments were used for the quantification. Representative images of AO-stained nuclei in the late pachytene/early diplotene region, where apoptosis occurs, are shown. Arrowheads indicate AO-stained nuclei.

(D) Percent embryonic lethality in wild-type (N2), *pig-1*, or *mes-2* mutants after treatment with 0, 60, or 120 Gy radiation. Synchronized young adult worms were treated with IR and rescued overnight, and eggs were collected from at least 15 worms for 4–6 hr. The average of at least three experiments is shown. Data are represented as means ± SD; $^{ns}p > 0.05$, *p < 0.05, **p < 0.01.

(E) Relative pig-1 and mes-2 mRNA expression after IR, normalized to untreated wild-type worms. Total RNA was extracted 4 hr after young adult worms were treated with 120 Gy IR. The graph is an average of at least three experiments performed on three separate days.

(F) Percent embryonic lethality in wild-type N2, *pig-1*, or *mes-2* mutant lines with or without pig-1 RNAi knockdown followed by IR. Synchronized L1 larvae were subjected to RNAi with pig-1 (RNAi) or control (RNAi) and treated with IR (60 Gy) as young adults. They were then rescued overnight and eggs were collected from at least 15 worms for 4–6 hr. The graph is an average of at least three experiments performed on three separate days, except for *mes-2 (bn11);* control (RNAi), which was repeated two times. Data are represented as means ± SD; $^{ns}p > 0.05$, *p < 0.05, **p < 0.01.

(G) Relative *mes-2* mRNA expression in N2 or *pig-1(gm344)* mutant. Data represent the mean ± SD; *p < 0.05; p values were calculated by Student's two-tailed t test. The graph is an average of at least three experiments performed on three separate days.

See also Figure S4.

The nematode *EZH2* homolog, MES-2, has an established role in the germline (Garvin et al., 1998; Holdeman et al., 1998), but the role of the *MELK* homolog, PIG-1, in germ cells is unknown. The presence of *pig-1* transcripts in the germline, as revealed by in situ hybridization (NEXT database, http://nematode.lab.nig.ac.jp/) and quantitative RT-PCR (qRT-PCR) analysis (Figure S4), suggests that *pig-1* is expressed in the germline. Therefore, we utilized a mutant strain containing the putative null allele *gm344*, which is a 524 bp deletion of the promoter region through part of the

second exon, to determine whether *pig-1* also has a functional role in germ cells. DAPI staining of *pig-1(gm344)* mutant germlines revealed a significant reduction in the number of proliferating mitotic cells compared with age-matched wild-type (N2) germlines (Figure 3B). *pig-1* also appears to negatively regulate germ cell apoptosis, as acridine orange (AO) staining showed that *pig-1(gm344)* animals had a modest but consistent increase in apoptosis compared with N2 animals (Figure 3C, compare the first and third bars). These data suggest that *pig-1* has conserved functions in cell proliferation and apoptosis (Gu et al., 2013; Joshi et al., 2013; Nakano et al., 2005, 2008, 2011).

When treated with IR, *C. elegans* germlines are known to activate protective mechanisms, including mitotic cell-cycle arrest, repair, and apoptosis. Therefore, we investigated the effect of IR on the survival of embryos from animals with genetic mutations in *pig-1* or *mes-2*. Young adult worms containing mature germlines were treated with varying doses of IR and the numbers of hatched and unhatched progeny were counted to determine the rate of embryonic lethality. Both *pig-1(gm344)* and *mes-2(bn11)* mutant animals showed a dose-dependent increase in embryonic lethality compared with wild-type control (N2) animals (Figure 3D). Apoptosis was also significantly higher in IR-treated *pig-1(gm344)* and *mes-2(bn11)* animals compared with IR-treated N2 animals (Figure 3C). Similar to what was observed for MELK, *pig-1* transcript levels increased after IR exposure (Figure 3E). These results indicate that loss of either *pig-1* or *mes-2* leads to a compromised response to IR exposure, resulting in increased germ cell apoptosis as well as higher rates of embryonic lethality.

Next, to determine whether *pig-1* and *mes-2* act in a common pathway or two parallel pathways, we investigated the genetic interactions between these genes using RNAi. A reduction of *pig-1* expression by RNAi resulted in hypersensitivity to IR to a degree similar to that observed in the *pig-1(gm344)* mutant (compare the second and third bars in Figure 3F), confirming that the IR-induced embryonic lethality observed in this mutant is due to the loss of *pig-1*. Downregulation of *pig-1* in both the N2 and *mes-2(bn11)* genetic backgrounds resulted in a similar percentage of embryonic lethality, suggesting that these two genes act in the same pathway (Figure 3F). In agreement with this, the level of *mes*-2 transcripts, as determined by qRT-PCR, was decreased in pig-1 mutant worms in comparison with N2 (Figure 3G). Together, these data indicate that the biological functions and the relationship of MELK and EZH2 are evolutionarily conserved.

EZH2 Is Transcriptionally Regulated by MELK in GBM Spheres

We then sought to determine how MELK is associated with EZH2 signaling in GSCs. When MELK was silenced in GBM83 spheres by shRNA, both the mRNA and protein expressions of EZH2 were significantly decreased (Figures 4A and 4B). However, mRNA expression was restored when *EZH2* was exogenously expressed in these MELK-silenced cells (Figure 4A). We performed a luciferase assay to assess the change in EZH2 promoter activity due to MELK overexpression in GBM83 spheres. Overexpression of MELK (coding region) increased EZH2 promoter activity, and in turn this increase was largely attenuated by either shRNA targeting the 3′ UTR of MELK (Figure 4C) or pharmacological treatment with Compound 1 (C1, a MELK inhibitor) (Figure 4D; Minata et al., 2014). Consistent with the change in *EZH2* mRNA expression and its promoter activity by MELK, flow cytometry with EZH2 antibody demonstrated that EZH2 protein expression was decreased when GBM83 spheres were passaged from serum-free neurosphere (NS) medium to prodifferentiation conditions (DC) (Figure 4E). This change in EZH2 expression was largely, but not completely, restored by MELK overexpression, whereas pretreatment with GSK126 (an EZH2 inhibitor) did not result in the same effect (Figure 4E). In turn, shRNA-mediated MELK silencing alone was sufficient to decreased EZH2 expression in GBM83 spheres, which was recovered by combined EZH2 overexpression. Collectively, these data suggest that EZH2 is transcriptionally regulated by MELK in GSCs.

EZH2 Is a Direct Target of the MELK/FOXM1 Complex in GBM Spheres

Since MELK is a protein kinase without DNA-binding domains, an intermediate transcription factor may be required to directly regulate the expression level of *EZH2* transcripts. Therefore, we aimed to identify the direct regulatory molecule for *EZH2* transcriptional activity in GSCs. Our recent studies identified novel cancer-specific substrates for MELK protein, including the Forkhead transcription factor FOXM1 (Joshi et al., 2013). Similar to what was observed for *MELK* and *EZH2* (Figure 1C), the expression profiles of *FOXM1* in GBM tumors exhibited a statistically significant correlation with those of *EZH2* (Figure 5A). The statistically significant correlation of *FOXM1* and *EZH2* expression in glioma tumors was also observed in other three data sets (Freije et al., 2004; Sun et al., 2006; Verhaak et al., 2010; https://tcga-data.nci.nih.gov/docs/publications/gbm_exp/) (Figure S5). In addition, *FOXM1* was significantly elevated in GBM patients with a worse prognosis (Figure 5B). Therefore, we hypothesized that FOXM1 may mediate the MELK-EZH2 signaling axis in GSCs. shRNA-mediated FOXM1 knockdown decreased *EZH2* mRNA expression in GBM83 cells, which was restored by *EZH2* exogenous expression (Figure 5C). In vitro luciferase reporter assay demonstrated that forced expression of FOXM1 increased EZH2 promoter activity

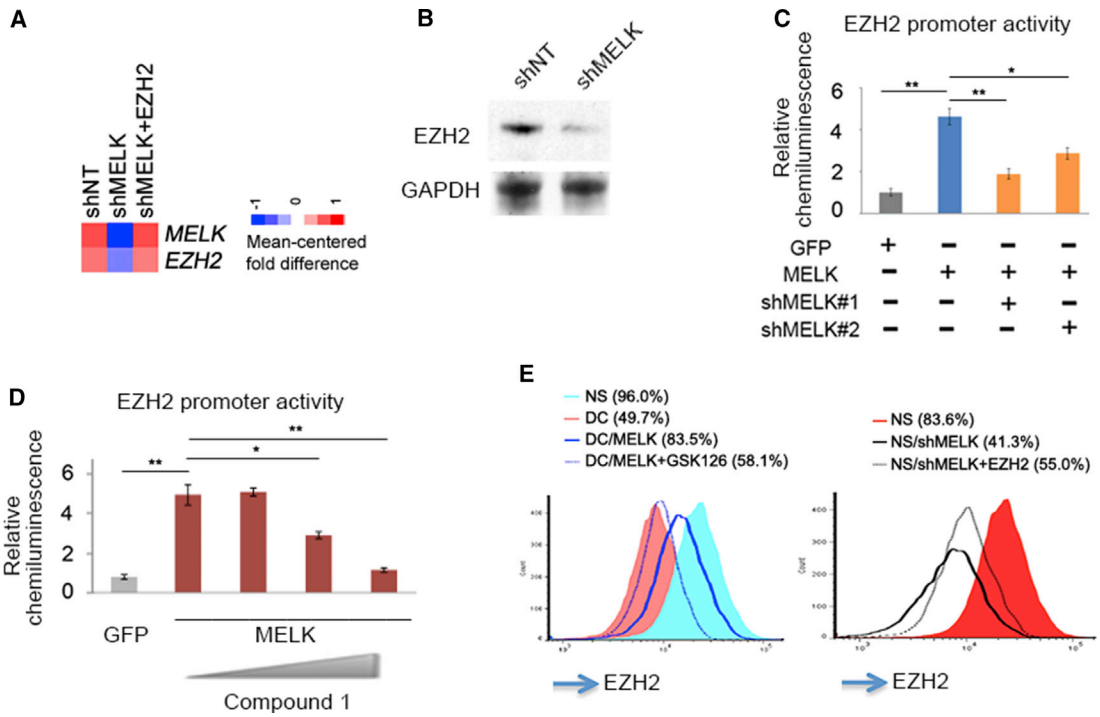

Figure 4. *EZH2* Is Transcriptionally Regulated by MELK in GBM Spheres

(A) Heatmap of *MELK* and *EZH2* expression in GBM83 spheres after treatment with shNT, shMELK, or shMELK plus EZH2 overexpression.

(B) Western blot for EZH2 in shMELK-infected GBM83 spheres. shNT was the control for MELK knockdown. GAPDH was the loading control.

(C) Relative chemiluminescence of luciferase driven by the *EZH2* promoter after infection of GBM spheres with GFP control, MELK overexpression vector, or MELK overexpression with shMELK. Data represent the mean ± SD of three independent experiments and statistical significance was evaluated by one-way ANOVA followed by Bonferroni post hoc tests. *$p < 0.05$; **$p < 0.01$.

(D) Relative chemiluminescence of EZH2 promoter activity in GBM spheres after infection with GFP control or MELK overexpression vector and increasing doses of the MELK inhibitor C1. Data represent the mean ± SD of three independent experiments and statistical significance was evaluated by one-way ANOVA followed by Bonferroni post hoc tests. *$p < 0.05$; **$p < 0.01$.

(E) Flow-cytometric analysis of GBM83 spheres in neurosphere (NS) or differentiation (DC) medium. Analysis of spheres in DC medium also included samples treated with MELK overexpression or MELK overexpression plus GSK126 (left panel). Spheres cultured in NS medium were also treated with shMELK or shMELK plus EZH2 overexpression vector.

in GBM83 spheres (Figure 5D). Of note, compared with MELK (Figure 4), FOXM1 had a 3-fold greater impact on *EZH2* promoter activity. MELK silencing by shRNA substantially diminished FOXM1-driven *EZH2* transcriptional activity, whereas FOXM1 silencing had only a marginal effect on MELK-driven *EZH2* transcriptional activity in GBM83 spheres. This result indicates that the action of FOXM1 largely depends on MELK, but not vice versa, for activation of the *EZH2* promoter in GSCs. The FOXM1-dependent transcriptional activity of *EZH2* was also confirmed by cotreatment with FOXM1 overexpression and the FOXM1 inhibitor siomycin A (Figure 5E). At the molecular level, both the MELK/FOXM1 protein complex and the kinase-dependent phosphorylation of FOXM1 were essential for FOXM1-driven transcriptional activation of EZH2, because MELK mutant protein lacking FOXM1 binding (D150A) and FOXM1 mutant protein lacking phosphorylation (596/678), but not transactivation (715/724) function, masked the transactivation of *EZH2* transcripts by MELK and FOXM1 (Figures 5F and 5G). These results indicate that binding of MELK to FOXM1 and subsequent phosphorylation of FOXM1 are essential for the transcriptional activation of *EZH2* in GSCs. We further confirmed that FOXM1 occupies the genomic region that regulates the EZH2 transcripts in GSCs by chromatin immunoprecipitation (ChIP)-PCR (Figure 5H). In turn, when these cells were pretreated with either MELK inhibitor (C1) or FOXM1 inhibitor (siomycin A) (Gartel, 2013), the occupancy of FOXM1 in the *EZH2* promoter was largely abolished, suggesting that the MELK-dependent FOXM1 signals to drive *EZH2* transcripts in GSCs (Figure 5I). To validate the MELK/FOXM1-mediated EZH2 signaling axis in GSCs, we performed a transcriptome microarray followed by qRT-PCR validation with GBM83

cells. As expected, all of the known EZH2 downstream target genes, except for *RUNX3*, were strongly suppressed by both MELK shRNA and FOXM1 shRNA, and the combined expression of EZH2 with knockdown of either MELK or FOXM1 restored their expression back to or nearly to the basal levels (Figure 5J). Consistent with these mRNA expression data, FACS analysis demonstrated that diminished *EZH2* expression in differentiated GBM83 spheres was partially restored by FOXM1 overexpression alone, but not when combined with GSK126 (Figure 5K). In turn, overexpression of both MELK and FOXM1 in these cells completely restored EZH2 expression only in the absence of GSK126, suggesting that in these GSC cultures, MELK and FOXM1 are the predominant regulators of EZH2 transcriptional expression. Similarly to MELK knockdown, FOXM1 knockdown significantly reduced EZH2 protein levels, and when FOXM1 knockdown was combined with exogenous expression of EZH2, the decrease in EZH2 was restored to near basal levels. Lastly, we investigated whether FOXM1 rescues IR-induced GSC apoptosis similarly to MELK, and whether GSK126 treatment could also mask this phenotype. As shown in Figure 5L, IR-induced apoptosis was largely rescued by FOXM1 overexpression, and cotreatment with GSK126 prevented apoptosis in these stem cell populations.

DISCUSSION

In this study, we report a number of findings: (1) in GBM tumors, MELK and EZH2 proteins are mostly colocalized in a subset of tumor cells; (2) the fraction of $MELK^+$ and $EZH2^+$ cells preferentially increases in postradio-/chemotherapy recurrent GBM tumors compared with de novo untreated tumors; (3) radioprotection of stem cells by the MELK-EZH2 axis is evolutionarily conserved between *C. elegans* and human; (4) in human GBM, GSC radioresistance depends largely on MELK-mediated EZH2 signaling in vitro, and MELK knockdown using shRNA radiosensitizes in vivo tumors; (5) *EZH2* is a direct target of the oncogenic transcription factor FOXM1 in GSCs; (6) signals derived from the MELK/FOXM1 protein complex are both sufficient and required to drive the transcriptional activity of *EZH2* in GSCs; and (7) clinically, MELK, FOXM1, and EZH2 are strongly linked to GBM patient prognosis.

Our data provide evidence that the oncogenic protein complex MELK/FOXM1 is a crucial transcriptional regulator of *EZH2*. EZH2, a lysine methyltransferase of PRC2, mediates the transcriptional repression of prodifferentiation genes in neoplastic stem cells (Margueron and Reinberg, 2011; Richly et al., 2011; Sparmann and van Lohuizen, 2006). While the oncogenic role of EZH2 in various cancers as a transcriptional silencer is well established, it remains elusive how the *EZH2* gene is transcriptionally regulated in GSCs and whether *EZH2* upregulation is associated with radioresistance of cancers. Recently, a few transcription activators, including E2F1, Sox4, and miR-101, were implicated in the transcriptional control of *EZH2* (Smits et al., 2010; Tiwari et al., 2013). However, whether these factors play a role in GBM and GSCs requires further investigation.

Using *C. elegans* as a model system, we also demonstrated that the functional relationship between MELK and EZH2 is evolutionarily conserved. While the role of MES-2 (ortholog of EZH2 in *C. elegans*) in germ cells has been previously described (Garvin et al., 1998; Holdeman et al., 1998), we show that the *pig-1* (ortholog of MELK in *C. elegans*) gene has a functional role in the *C. elegans* germline. We found that the loss of *pig-1* resulted in a significant decrease in the number of proliferating mitotic cells, as well as an increase in apoptosis under physiological conditions. Previously, *pig-1* was implicated in the regulation of the developmental cell death pathway in young larvae and embryos (Chien et al., 2013; Cordes et al., 2006). In this context, *pig-1* supports apoptosis in somatic cells, suggesting that *pig-1* may have opposite roles in somatic versus germ cells or in cells with diverse differentiation states, as also suggested by several studies in mammalian cells (Joshi et al., 2013; Nakano et al., 2005). Furthermore, *pig-1* and *mes-2* mutant animals showed an increase in both the rate of apoptosis and embryonic lethality after IR in comparison with wild-type worms. A genetic interaction analysis suggested that *pig-1* and *mes-2* act through a common pathway and that mes-2 mRNA levels are decreased in *pig-1* mutant animals. Although the lack of a clear FOXM1 homolog in *C. elegans* prevented further analysis of MELK/EZH2 signaling in the nematode, the data support the results obtained with MELK and EZH2 in human GSCs.

An important therapeutic implication of the present data is derived from the impact of MELK knockdown when combined with IR for GSC-derived mouse xenografted tumors. For decades, IR has been a mainstay of treatment for GBM patients; however, the exact molecular mechanisms that drive GBM radioresistance remain unclear. Our data indicate that after IR, GSCs may become more dependent on MELK-driven FOXM1/EZH2 signaling, raising the possibility of novel therapeutic approaches for GBM. EZH2 and FOXM1 are both oncogenic proteins with substantially elevated expression in various cancers, including GBM. Nonetheless, it is extremely challenging to develop molecularly targeted therapeutics for transcription factors. There are no established EZH2 targeting therapies for any cancer, but a phase I clinical trial (NCT02082977) using an EZH2 inhibitor, GSK2816126 (an analog of GSK126 used in this study), for relapsed/refractory diffuse large B cell and transformed follicular

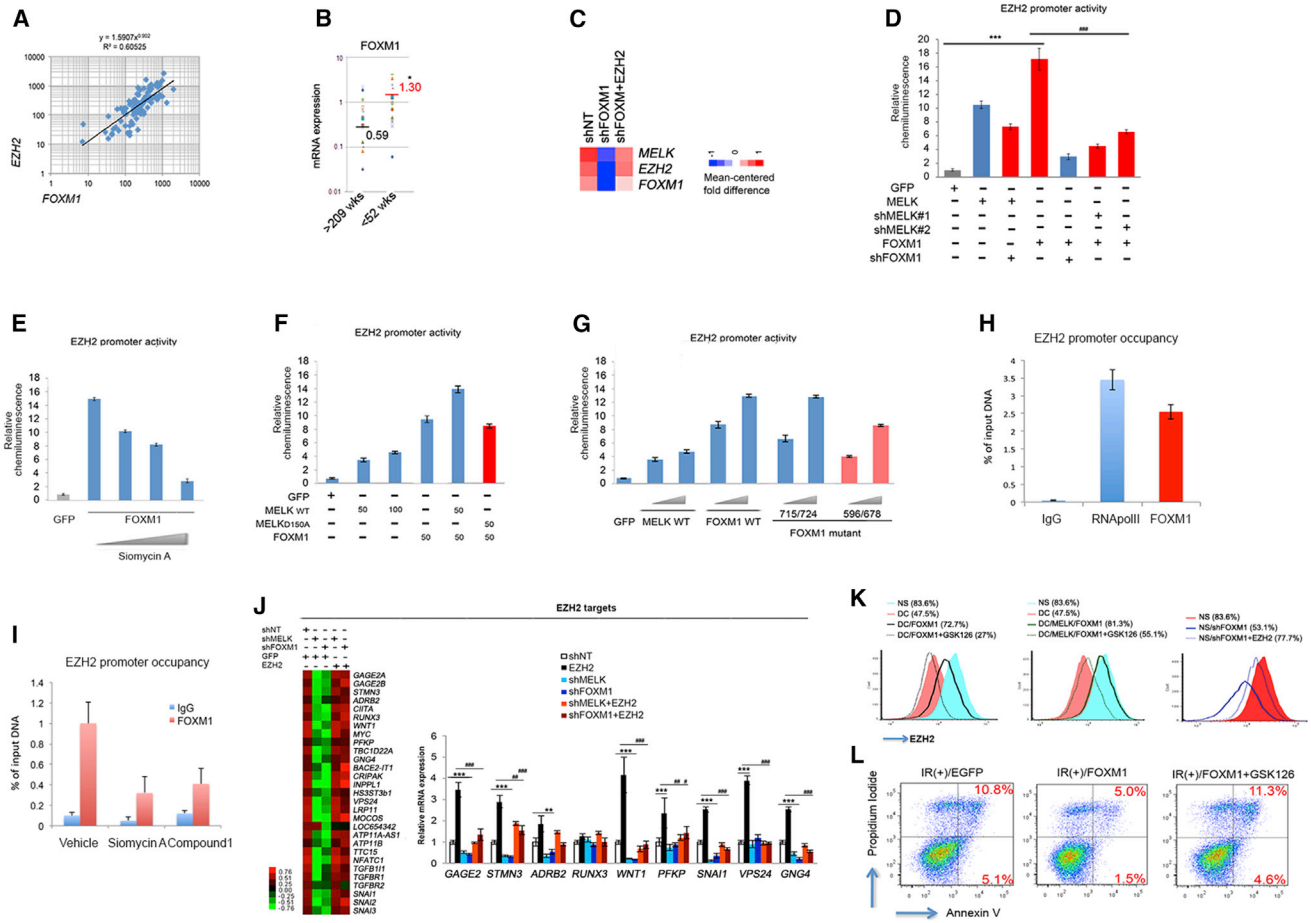

Figure 5. *EZH2* Is a Direct Target of the MELK/FOXM1 Complex in GBM Spheres

(A) Correlation of *FOXM1* and *EZH2* mRNA expression by microarray analysis of HGGs (n = 76).

(B) *FOXM1* mRNA expression in patients with good (>209 weeks survival, n = 19) versus poor (<52 weeks survival, n = 17) prognosis in the Phillips et al. (2006) data set. Asterisk (*) indicates statistical significance by Student's two-tailed t test. *p < 0.05.

(C) Heatmap of *MELK, EZH2*, and *FOXM1* expression in GSCs after treatment with shNT control, shFOXM1, or shFOXM1 plus EZH2 overexpression.

(D) Relative chemiluminescence of luciferase driven by the *EZH2* promoter after infection of GBM spheres with GFP control, MELK overexpression vector, or FOXM1 overexpression vector. MELK overexpression treatment was also combined with shFOXM1, and FOXM1 overexpression treatment was also combined with shMELK or shFOXM1. Data represent the mean ± SD from three independent experiments and statistical significance was evaluated by one-way ANOVA followed by Bonferroni post hoc tests. GFP versus MELK, MELK+shFOXM1, or FOXM1: ***p < 0.001; FOXM1 versus FOXM1+shFOXM1, FOXM1+shMELK#1, or FOXM1+shMELK#2: $^{###}$p < 0.001.

(E) Relative chemiluminescence of EZH2 promoter activity in GBM spheres after infection with GFP control or FOXM1 overexpression vector and increasing doses of the FOXM1 inhibitor siomycin A (0.05–0.5 μM). Data represent the mean ± SD of triplicate experiments.

(F) Relative chemiluminescence of EZH2 promoter activity in GBM spheres after infection with GFP control or combinations of MELK wild-type (WT) overexpression, FOXM1 binding-deficient MELK (MELK D150A), or FOXM1 overexpression. Data represent the mean ± SD of triplicate experiments.

(G) Relative chemiluminescence of EZH2 promoter activity in GBM spheres after infection with GFP control or MELK, FOXM1 WT, and FOXM1 mutated overexpression vectors with increasing doses of the MELK inhibitor C1. Data represent the mean ± SD of triplicate experiments.

(H) ChIP for RNA pol II or FOXM1 followed by PCR for the *EZH2* promoter. Data represent the mean ± SD of triplicate experiments. A representative data set from three independent experiments is shown.

(I) ChIP for FOXM1 or IgG control at the *EZH2* promoter after pretreatment of spheres with vehicle control, siomycin A, or C1. Data represent the mean ± SD of triplicate experiments. A representative data set from three independent experiments is shown.

(J) Microarray analysis and qPCR validation of EZH2 targets in GSCs treated with shNT (control), shMELK, shFOXM1, and EZH2 overexpression. The gene expression levels were validated by real-time RT-PCR. Data represent the mean ± SD from three independent

(legend continued on next page)

lymphoma is currently ongoing. Our identification of the protein kinase MELK as a key regulator of FOXM1-driven EZH2 signaling in preclinical GBM tumors and GSCs may facilitate the development of MELK-targeted therapies that can lead to FOXM1/EZH2 deregulation in GBM. In 2013, a phase I clinical trial (NCT01910545) for non-CNS cancers was started in order to test OTS167, a small-molecule kinase inhibitor with high specificity for MELK. Recently, we also identified C1 as a kinase inhibitor that preferentially inhibits MELK (Minata et al., 2014). Given that MELK knockdown strongly sensitizes GSC-derived mouse tumors to IR, it is an attractive idea to combine IR therapy with chemotherapy using a MELK inhibitor (and possibly an EZH2 inhibitor) for GBM.

Our results suggest several open questions that will require further investigation. Although evidence suggests that eradication of cancer stem cells appears to be beneficial for curing cancers, recent studies also suggest that non-cancer stem cells acquire a cancer stem cell phenotype when challenged by stressors such as glucose deprivation (Flavahan et al., 2013). Thus, eradication of the existing cancer stem cells may not be sufficient, and instead a therapeutic combination targeting noncancer stem cells in addition to cancer stem cells may be mandatory. The IR-induced increases in MELK and EZH2 may be due to (1) the preferential eradication of nonstem tumor cells and subsequent enrichment of GSCs after treatment (i.e., selection of a therapy-resistant tumor cell population) or (2) IR-induced phenotypic changes of the treated GBM sphere cells, resulting in increased MELK and subsequently EZH2 through modulation of stress-induced enzymes (plasticity of GSCs and non-GSCs). It is also possible that both explanations are true. Future studies will address this issue.

Another open question is, which GBM subtypes and GSC subtypes are dependent on the MELK-FOXM1-EZH2 signaling axis? Thus far, recent genome-wide transcriptome and methylome analyses support the existence of three to six GBM subtypes (Phillips et al., 2006; Sturm et al., 2012; Verhaak et al., 2010) and two GSC subtypes (Bhat et al., 2013; Mao et al., 2013). It is not entirely clear whether any of the GBM/GSC subtypes are more preferentially dependent on the MELK-FOXM1-EZH2 axis or all subtypes rely equally on this signaling axis. Future studies will address this question.

In conclusion, in this study, we identified a signaling pathway for EZH2 upregulation in GSCs that plays a critical role in GBM tumor propagation and radioresistance. Identification of the MELK/FOXM1 protein complex as the predominant regulator for the *EZH2* gene in GSCs highlights a possible therapeutic target for the devastating disease GBM.

EXPERIMENTAL PROCEDURES

Glioma Tumor-Derived Neurospheres

All of the work related to human tissues was performed at The Ohio State University and MD Anderson Cancer Center under institutional review board-approved protocols according to NIH guidelines. Glioma and normal neurospheres were derived from 19 HGG samples, three fetal-brain-derived astrocytes, and neural progenitors as described previously (Bhat et al., 2013; Gu et al., 2013; Guvenc et al., 2013; Miyazaki et al., 2012; Nakano et al., 2011). For the Ohio State University samples, brain tumor resections were performed by Drs. I. Nakano and E.A. Chiocca (Department of Neurological Surgery, The Ohio State University). In brief, freshly resected glioma tumor samples were dissociated into single cells using both mechanical (neurospheres were gently pipetted with P1000 pipet tips four to five times) and enzymatic (TrypLE Express; Invitrogen) methods. The dissociated tumor cells were cultured in Dulbecco's modified Eagle's medium (DMEM)/F12 (Invitrogen) supplemented with B27 (1:50), heparin (5 mg/ml), basic fibroblast growth factor (bFGF; 20 ng/ml), and epidermal growth factor (EGF; 20 ng/ml). Growth factors (bFGF and EGF) were added twice a week. For differentiation of GSCs, neurospheres were cultured in DMEM/F12 supplemented with 10% (vol/vol) fetal bovine serum for 10 days. All of the neurospheres analyzed in this study were cultured for <20 passages from surgery or xenograft mouse intracranial tumors. In some experiments, various neurospheres were exposed to radiation after cells were plated at a density of 1×10^6 cells/flask 1 day before radiation treatment.

Gene Expression Omnibus Profile and TCGA

MELK and FOXM1 expression data (Affymetrix Human Genome U133A Array) were downloaded from the GDS1815 data set and analyzed for grade III glioma and GBM. The Cancer Genome Atlas

experiments and statistical significance was evaluated by one-way ANOVA followed by Bonferroni post hoc tests. shNT versus EZH2, shMELK, or shFOXM1: $^{**}p < 0.01$,$^{***}p < 0.001$; EZH2 versus shMELK+EZH2 or shFOXM1+EZH2: $^{\#}p < 0.05$, $^{\#\#}p < 0.01$, $^{\#\#\#}p < 0.001$.

(K) Flow-cytometric analysis for EZH2 of glioma spheres cultured in neurosphere (NS) or differentiation (DC) medium. Analysis of spheres in DC medium also included samples treated with FOXM1 overexpression with or without GSK126 (left panel), and MELK and FOXM1 overexpression with or without GSK126 (middle panel). Spheres cultured in NS medium were also treated with shFOXM1 or shFOXM1 plus EZH2 overexpression vector (right panel).

(L) Flow-cytometric analysis of irradiated GBM spheres for Annexin V and propidium iodide. Irradiated spheres were treated with either EGFP control (left panel), FOXM1 overexpression vector (middle panel), or FOXM1 overexpression with GSK126 (right panel).

See also Figure S5.

(TCGA) data are available through the TCGA Data Portal at https://tcga-data.nci.nih.gov/tcga/.

ChIP-PCR Analysis to Determine *EZH2* Promoter Occupancy

Using the Genomatrix program, we searched the consensus binding site in the human EZH2 promoter and performed ChIP-PCR using the QIAGEN ChIP kit according to the manufacturer's protocol. A total of 131 patient-derived GBMs were treated with either C1 or siomycin A for 1 day and processed for genomic DNA isolation.

C. elegans Culture and Strains

C. elegans worms were grown at 20°C on nematode growth medium (NGM) plates seeded with OP50 *E. coli* bacteria under standard laboratory conditions (Brenner, 1974) unless otherwise indicated.

The strains used in this study were obtained from the *C. elegans* Genetic Center and included N2 Bristol (wild-type), NG4370 *zdIs5*; *pig-1 (gm344)* IV, and SS186 *mes-2 (bn11), unc-4 (e120)/mnC1, dpy-10 (e128), unc-52 (e444)* II.

RNAi for *C. elegans*

RNAi experiments were performed using the feeding method described in (Timmons, 2006). N2 worms were fed HT115 bacteria strains containing *pig-1* RNAi from the Ahringer library (Kamath et al., 2003) or HT115 bacteria containing the empty L4440 feeding vector as a control. Bacteria were applied to plates containing 1 mM isopropyl β-d-thiogalactoside (Sigma Aldrich) and 50 μg/ml ampicillin (Sigma Aldrich), and induced overnight at room temperature. Synchronized L1 animals were put on the plates, grown until young adulthood (20–24 hr after L4), and then used for embryonic lethality experiments (see below).

The graph in Figure 3E is an average of at least three experiments performed on three separate days, except for the *mes-2 (bn11)*; control (RNAi) experiment, which was repeated two times.

Embryonic Lethality Assay in *C. elegans*

Synchronized young adult worms (20–24 hr after L4 stage) were treated with the indicated amounts of ionizing IR (Faxitron X-ray machine) and allowed to recover for 24 hr. Thirty worms for each variable were divided into ten worms/three plates and allowed to lay eggs for 4–6 hr. After 24–48 hr, hatched and unhatched progeny were counted with the use of a dissecting microscope to determine the percentage of embryonic lethality (unhatched eggs/total progeny). The experiment was performed in triplicate on three separate days.

Quantification of Apoptosis in *C. elegans*

Apoptotic germlines were scored in young adult worms 24 hr after IR treatment or in age-matched untreated controls using AO (10 mg/ml; Molecular Probes) staining as described previously (Craig et al., 2012). In brief, worms were removed from plates with M9 buffer into a microfuge tube. Then, 200 μl of AO (5 μL/ml) was added and the tubes were covered in foil and incubated for 2 hr. The worms were placed on NGM plates with food and then on slides with agarose pads. AO^+ cells were counted using the 40× objective on a fluorescence microscope (Zeiss Imager M2).

Quantification of Mitotic Cells in *C. elegans*

Synchronized young adult *pig-1* and N2 worms grown at 25°C were fixed with methanol/acetone and stained with DAPI (100 ng/ml in PBST). In brief, the worms were washed from the plates with M9 buffer and incubated in −20°C methanol for 10 min, incubated in −20°C acetone for 5 min, washed one time in PBST, incubated for 10 min in DAPI at room temperature, and washed two times in PBST. Images of germlines were acquired with a 60× objective on a fluorescence microscope (Zeiss Imager M2) and the mitotic nuclei of optically bisected germlines were counted with the use of ImageJ Micromanager software. Two independent experiments were used for quantification.

The experimental methods used in this work are detailed in the Supplemental Experimental Procedures.

ACCESSION NUMBERS

The NCBI Gene Expression Omnibus accession number for the microarray data reported in this paper is GSE63963.

SUPPLEMENTAL INFORMATION

Supplemental Information includes Supplemental Experimental Procedures and five figures and can be found with this article online at http://dx.doi.org/10.1016/j.stemcr.2014.12.006.

AUTHOR CONTRIBUTIONS

S.-H.K., K.J., J.L., K.P.L.B., T.M., A.E.S., and I.N. designed experiments. S.-H.K., K.J., J.S., R.T., C.G., L.C., R.W., T.R.M., and K.P.L.B. performed research. S.-H.K., J.S., M.N.-O., M.M., E.P.S., J.L., K.P.L.B., T.M., A.E.S., and I.N. analyzed the data. E.P.S. provided samples. S.-H.K., J.S., A.E.S., and I.N. wrote the manuscript.

ACKNOWLEDGMENTS

We thank Dr. Jeremy Rich (CCF) for constructive discussions during this study. *C. elegans* strains were provided by the CGC, which is funded by NIH Office of Research Infrastructure Programs (P40 OD010440). This work was supported by grants from the American Cancer Society (MRSG-08-108-01), the NIH (NIH/NCI P01 CA163205, R21 CA175875, NIH/NINDS R01 NS083767, and R01 NS087913 to I.N., and R01 NS082312 to J.L.), the Danish Cancer Society (KB30826 to T.R.M.), and the Danish National Research Foundation (DNRF82 to A.E.S.).

Received: June 17, 2014
Revised: December 8, 2014
Accepted: December 9, 2014
Published: January 15, 2015

REFERENCES

Aloia, L., Di Stefano, B., and Di Croce, L. (2013). Polycomb complexes in stem cells and embryonic development. Development *140*, 2525–2534.

Bao, S., Wu, Q., McLendon, R.E., Hao, Y., Shi, Q., Hjelmeland, A.B., Dewhirst, M.W., Bigner, D.D., and Rich, J.N. (2006). Glioma stem cells promote radioresistance by preferential activation of the DNA damage response. Nature *444*, 756–760.

Bhat, K.P., Balasubramaniyan, V., Vaillant, B., Ezhilarasan, R., Hummelink, K., Hollingsworth, F., Wani, K., Heathcock, L., James, J.D., Goodman, L.D., et al. (2013). Mesenchymal differentiation mediated by NF-κB promotes radiation resistance in glioblastoma. Cancer Cell *24*, 331–346.

Brennan, C.W., Verhaak, R.G., McKenna, A., Campos, B., Noushmehr, H., Salama, S.R., Zheng, S., Chakravarty, D., Sanborn, J.Z., Berman, S.H., et al.; TCGA Research Network (2013). The somatic genomic landscape of glioblastoma. Cell *155*, 462–477.

Brenner, S. (1974). The genetics of *Caenorhabditis elegans*. Genetics *77*, 71–94.

Chien, S.C., Brinkmann, E.M., Teuliere, J., and Garriga, G. (2013). Caenorhabditis elegans PIG-1/MELK acts in a conserved PAR-4/LKB1 polarity pathway to promote asymmetric neuroblast divisions. Genetics *193*, 897–909.

Cordes, S., Frank, C.A., and Garriga, G. (2006). The C. elegans MELK ortholog PIG-1 regulates cell size asymmetry and daughter cell fate in asymmetric neuroblast divisions. Development *133*, 2747–2756.

Craig, A.L., Moser, S.C., Bailly, A.P., and Gartner, A. (2012). Methods for studying the DNA damage response in the *Caenorhabdatis elegans* germ line. Methods Cell Biol. *107*, 321–352.

Flavahan, W.A., Wu, Q., Hitomi, M., Rahim, N., Kim, Y., Sloan, A.E., Weil, R.J., Nakano, I., Sarkaria, J.N., Stringer, B.W., et al. (2013). Brain tumor initiating cells adapt to restricted nutrition through preferential glucose uptake. Nat. Neurosci. *16*, 1373–1382.

Freije, W.A., Castro-Vargas, F.E., Fang, Z., Horvath, S., Cloughesy, T., Liau, L.M., Mischel, P.S., and Nelson, S.F. (2004). Gene expression profiling of gliomas strongly predicts survival. Cancer Res. *64*, 6503–6510.

Gartel, A.L. (2013). Thiazole antibiotics siomycin and thiostrepton inhibit the transcriptional activity of FOXM1. Front. Oncol. *3*, 150.

Garvin, C., Holdeman, R., and Strome, S. (1998). The phenotype of mes-2, mes-3, mes-4 and mes-6, maternal-effect genes required for survival of the germline in Caenorhabditis elegans, is sensitive to chromosome dosage. Genetics *148*, 167–185.

Gu, C., Banasavadi-Siddegowda, Y.K., Joshi, K., Nakamura, Y., Kurt, H., Gupta, S., and Nakano, I. (2013). Tumor-specific activation of the C-JUN/MELK pathway regulates glioma stem cell growth in a p53-dependent manner. Stem Cells *31*, 870–881.

Guvenc, H., Pavlyukov, M.S., Joshi, K., Kurt, H., Banasavadi-Siddegowda, Y.K., Mao, P., Hong, C., Yamada, R., Kwon, C.H., Bhasin, D., et al. (2013). Impairment of glioma stem cell survival and growth by a novel inhibitor for Survivin-Ran protein complex. Clin. Cancer Res. *19*, 631–642.

Hemmati, H.D., Nakano, I., Lazareff, J.A., Masterman-Smith, M., Geschwind, D.H., Bronner-Fraser, M., and Kornblum, H.I. (2003). Cancerous stem cells can arise from pediatric brain tumors. Proc. Natl. Acad. Sci. USA *100*, 15178–15183.

Holdeman, R., Nehrt, S., and Strome, S. (1998). MES-2, a maternal protein essential for viability of the germline in Caenorhabditis elegans, is homologous to a Drosophila Polycomb group protein. Development *125*, 2457–2467.

Joshi, K., Banasavadi-Siddegowda, Y., Mo, X., Kim, S.H., Mao, P., Kig, C., Nardini, D., Sobol, R.W., Chow, L.M., Kornblum, H.I., et al. (2013). MELK-dependent FOXM1 phosphorylation is essential for proliferation of glioma stem cells. Stem Cells *31*, 1051–1063.

Kamath, R.S., Fraser, A.G., Dong, Y., Poulin, G., Durbin, R., Gotta, M., Kanapin, A., Le Bot, N., Moreno, S., Sohrmann, M., et al. (2003). Systematic functional analysis of the *Caenorhabditis elegans* genome using RNAi. Nature *421*, 231–237.

Kim, E., Kim, M., Woo, D.H., Shin, Y., Shin, J., Chang, N., Oh, Y.T., Kim, H., Rheey, J., Nakano, I., et al. (2013). Phosphorylation of EZH2 activates STAT3 signaling via STAT3 methylation and promotes tumorigenicity of glioblastoma stem-like cells. Cancer Cell *23*, 839–852.

Lee, J., Son, M.J., Woolard, K., Donin, N.M., Li, A., Cheng, C.H., Kotliarova, S., Kotliarov, Y., Walling, J., Ahn, S., et al. (2008). Epigenetic-mediated dysfunction of the bone morphogenetic protein pathway inhibits differentiation of glioblastoma-initiating cells. Cancer Cell *13*, 69–80.

Mao, P., Joshi, K., Li, J., Kim, S.H., Li, P., Santana-Santos, L., Luthra, S., Chandran, U.R., Benos, P.V., Smith, L., et al. (2013). Mesenchymal glioma stem cells are maintained by activated glycolytic metabolism involving aldehyde dehydrogenase 1A3. Proc. Natl. Acad. Sci. USA *110*, 8644–8649.

Margueron, R., and Reinberg, D. (2011). The Polycomb complex PRC2 and its mark in life. Nature *469*, 343–349.

Minata, M., Gu, C., Joshi, K., Nakano-Okuno, M., Hong, C., Nguyen, C.H., Kornblum, H.I., Molla, A., and Nakano, I. (2014). Multi-kinase inhibitor C1 triggers mitotic catastrophe of glioma stem cells mainly through MELK kinase inhibition. PLoS ONE *9*, e92546.

Miyazaki, T., Pan, Y., Joshi, K., Purohit, D., Hu, B., Demir, H., Mazumder, S., Okabe, S., Yamori, T., Viapiano, M., et al. (2012). Telomestatin impairs glioma stem cell survival and growth through the disruption of telomeric G-quadruplex and inhibition of the proto-oncogene, c-Myb. Clin. Cancer Res. *18*, 1268–1280.

Nakano, I., Paucar, A.A., Bajpai, R., Dougherty, J.D., Zewail, A., Kelly, T.K., Kim, K.J., Ou, J., Groszer, M., Imura, T., et al. (2005). Maternal embryonic leucine zipper kinase (MELK) regulates multipotent neural progenitor proliferation. J. Cell Biol. *170*, 413–427.

Nakano, I., Masterman-Smith, M., Saigusa, K., Paucar, A.A., Horvath, S., Shoemaker, L., Watanabe, M., Negro, A., Bajpai, R., Howes, A., et al. (2008). Maternal embryonic leucine zipper kinase is a key regulator of the proliferation of malignant brain tumors, including brain tumor stem cells. J. Neurosci. Res. *86*, 48–60.

Nakano, I., Joshi, K., Visnyei, K., Hu, B., Watanabe, M., Lam, D., Wexler, E., Saigusa, K., Nakamura, Y., Laks, D.R., et al. (2011). Siomycin A targets brain tumor stem cells partially through a MELK-mediated pathway. Neuro-oncol. *13*, 622–634.

Phillips, H.S., Kharbanda, S., Chen, R., Forrest, W.F., Soriano, R.H., Wu, T.D., Misra, A., Nigro, J.M., Colman, H., Soroceanu, L., et al. (2006). Molecular subclasses of high-grade glioma predict prognosis, delineate a pattern of disease progression, and resemble stages in neurogenesis. Cancer Cell *9*, 157–173.

Radulović, V., de Haan, G., and Klauke, K. (2013). Polycomb-group proteins in hematopoietic stem cell regulation and hematopoietic neoplasms. Leukemia *27*, 523–533.

Richly, H., Aloia, L., and Di Croce, L. (2011). Roles of the Polycomb group proteins in stem cells and cancer. Cell Death Dis. *2*, e204.

Singh, S.K., Hawkins, C., Clarke, I.D., Squire, J.A., Bayani, J., Hide, T., Henkelman, R.M., Cusimano, M.D., and Dirks, P.B. (2004). Identification of human brain tumour initiating cells. Nature *432*, 396–401.

Smits, M., Nilsson, J., Mir, S.E., van der Stoop, P.M., Hulleman, E., Niers, J.M., de Witt Hamer, P.C., Marquez, V.E., Cloos, J., Krichevsky, A.M., et al. (2010). miR-101 is down-regulated in glioblastoma resulting in EZH2-induced proliferation, migration, and angiogenesis. Oncotarget *1*, 710–720.

Sparmann, A., and van Lohuizen, M. (2006). Polycomb silencers control cell fate, development and cancer. Nat. Rev. Cancer *6*, 846–856.

Sturm, D., Witt, H., Hovestadt, V., Khuong-Quang, D.A., Jones, D.T., Konermann, C., Pfaff, E., Tönjes, M., Sill, M., Bender, S., et al. (2012). Hotspot mutations in H3F3A and IDH1 define distinct epigenetic and biological subgroups of glioblastoma. Cancer Cell *22*, 425–437.

Sun, L., Hui, A.M., Su, Q., Vortmeyer, A., Kotliarov, Y., Pastorino, S., Passaniti, A., Menon, J., Walling, J., Bailey, R., et al. (2006). Neuronal and glioma-derived stem cell factor induces angiogenesis within the brain. Cancer Cell *9*, 287–300.

Timmons, L. (2006). Delivery methods for RNA interference in *C. elegans*. Methods Mol. Biol. *351*, 119–125.

Tiwari, N., Tiwari, V.K., Waldmeier, L., Balwierz, P.J., Arnold, P., Pachkov, M., Meyer-Schaller, N., Schübeler, D., van Nimwegen, E., and Christofori, G. (2013). Sox4 is a master regulator of epithelial-mesenchymal transition by controlling Ezh2 expression and epigenetic reprogramming. Cancer Cell *23*, 768–783.

Verhaak, R.G., Hoadley, K.A., Purdom, E., Wang, V., Qi, Y., Wilkerson, M.D., Miller, C.R., Ding, L., Golub, T., Mesirov, J.P., et al.; Cancer Genome Atlas Research Network (2010). Integrated genomic analysis identifies clinically relevant subtypes of glioblastoma characterized by abnormalities in PDGFRA, IDH1, EGFR, and NF1. Cancer Cell *17*, 98–110.